Field effect transistors with layered two-dimensional $SnS_{2-x}Se_x$ conduction channels: Effects of selenium substitution

T. S. Pan,[1,2,a)] D. De,[1,a)] J. Manongdo,[3,4] A. M. Guloy,[3] V. G. Hadjiev,[5] Y. Lin,[2,b)] and H. B. Peng[1,b)]
[1]Department of Physics and Texas Center for Superconductivity, University of Houston, Texas 77204-5005, USA
[2]State Key Laboratory of Electronic Thin Films and Integrated Devices, University of Electronic Science and Technology of China, Chengdu 610054, China
[3]Department of Chemistry and Texas Center for Superconductivity, University of Houston, Texas 77204-5003, USA
[4]Institute of Chemistry, University of the Philippines, Diliman, 1101 Quezon City, Philippines
[5]Department of Mechanical Engineering and Texas Center for Superconductivity, University of Houston, Texas 77204-5002, USA

(Received 22 May 2013; accepted 29 July 2013; published online 28 August 2013)

A thorough characterization of field effect transistors with conduction channels made of $SnS_{2-x}Se_x$ nanocrystals having different selenium content is presented. The main effect of increasing the selenium content is a suppression of the drain-source current modulation by the gate voltage. The temperature dependence of $SnS_{2-x}Se_x$ conductivity for all compositions is characterized by an activation energy that gradually decreases with x. A simple donor model, with parameters of SnS_2 and $SnSe_2$ deduced from density functional theory, suggests that the change in the activation energy is mostly due to enhanced dielectric constants that accompany the band gap reduction in $SnS_{2-x}Se_x$. © *2013 AIP Publishing LLC*. [http://dx.doi.org/10.1063/1.4819072]

Sustaining Moore's Law beyond silicon-based electronic devices has drawn ever-increasing attention on novel low-dimensional materials suitable for the production of field effect transistors (FETs), the building blocks for electronics. The discovery of graphene, a truly two-dimensional material comprised of atomically thin layer of carbon, has brought significant excitement and promises for novel applications.[1–5] Nevertheless, the range of application for graphene in digital electronics is limited by its absence of a band gap. As an alternative, other layered materials with a finite band gap such as boron nitrides, metal dichalcogenides, and molybdenum oxide have been considered.[6–9] Metal dichalcogenides provide promising materials for wide range of applications in areas like field effect devices,[10,11] memory devices,[12] and energy storage.[13,14] Among this class of materials, SnS_2, a semiconductor with a band gap of 2.1 eV, was recently shown to exhibit a high FET on/off ratio of $\sim 10^6$,[15] a feature much desirable for the next generation electronic devices.[16] Moreover, selenium doping in SnS_2 offers a useful route for bandgap engineering, in that the band gap of $SnS_{2-x}Se_x$ can be continuously tuned from 2.1 eV (SnS_2) to 1.0 eV ($SnSe_2$) by varying the selenium content.[17] This would provide an important versatility in low-power electronic and optoelectronic devices. For example, the bandgap of $SnSe_2$ is very close to that of silicon (1.1 eV), and was reported to have higher carrier mobility than SnS_2 in bulk form.[18] Therefore, a systematic study of FET devices based on nano-sized $SnS_{2-x}Se_x$ crystals as conduction channels will be very useful for evaluating the potential of these materials in future nanoelectronics applications.

Layered tin dichalcogenides, SnS_2 and $SnSe_2$, are both isostructural with the hexagonal CdI_2 type crystal structure and exhibit indirect band gaps.[19] Their valence bands are predominantly derived from the p orbitals of chalcogens (sulfur and/or selenium), whereas the conduction bands are hybridized orbitals derived from the p orbitals of the chalcogens (sulfur and/or selenium) and the s orbital of tin. Since both sulfur and selenium are group VI elements, a solid solution of the isostructural tin dichalcogenides, $SnS_{2-x}Se_x$ can be prepared. FET devices based on solution-processed granular thin films of $SnS_{2-x}Se_x$ exhibit larger current densities and relatively higher mobility compared with its analogous organic FETs.[10] However, there has been little work done on nano-sized crystalline $SnS_{2-x}Se_x$ as an effective conduction channel in FETs.

In this work, we investigated field-effect transistors based on mechanically exfoliated (11–35 nm thick) $SnS_{2-x}Se_x$ crystals with varying selenium content, systematically from $x = 0$ to 2. The FET characteristics were measured with temperature varied from 90 K to 295 K, and the activation energies are subsequently obtained as a function of selenium doping.

In our studies, bulk $SnS_{2-x}Se_x$ single crystals were grown by reacting the pure elements in quartz ampoules via chemical vapor transport using iodine as transport agent,[20] as described in a previous work.[15] Vacuum evacuated ampoules loaded with source materials were heated in a two-zone furnace and the as-grown crystals were transported from the hot zone (700 °C) to the cold zone (650 °C) over 12 h. Thereafter, the furnace was air-cooled to room temperature. Single crystals of the tin dichalcogenides, with six different compositions (SnS_2, $SnS_{1.6}Se_{0.4}$, $SnS_{1.2}Se_{0.8}$, $SnS_{0.8}Se_{1.2}$, $SnS_{0.4}Se_{1.6}$, and $SnSe_2$) were prepared, and their crystal structures were confirmed by X-ray diffraction (XRD)

a)T. S. Pan and D. De contributed equally to this work.
b)Author to whom correspondence should be addressed. Electronic addresses: linyuan@uestc.edu.cn and haibingpeng@uh.edu

 © 2013 AIP Publishing LLC

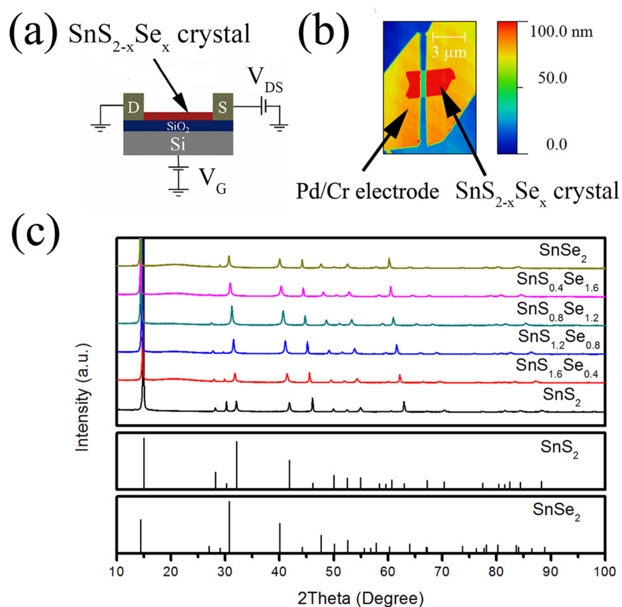

FIG. 1. (a) The schematic diagram of the field-effect device structure. (b) An atomic force microscopy (AFM) image of a $SnS_{2-x}Se_x$ device with x = 0.4. (c) The x-ray diffraction data of $SnS_{2-x}Se_x$ bulk compounds under study (upper panel) and the reference data (lower panels) of Refs. 21 and 22.

(PANalytical X'Pert PRO, Cu Kα, $\lambda = 1.5406$ Å). Subsequently, Scotch-tape method[15] was employed to mechanically exfoliate the $SnS_{2-x}Se_x$ crystals into thin nanocrystals. The device structure schematic and an atomic force microscope (AFM) image of a real FET device are shown in Figs. 1(a) and 1(b). Here the gate dielectrics consists of a 200-nm-thick SiO_2 layer deposited on doped Si wafer, and the source and drain electrodes are thermally-evaporated metal electrodes (45 nm Pd/5 nm Cr) connecting a thin $SnS_{2-x}Se_x$ nanocrystal (the FET conduction channel). All electrical measurements were conducted under vacuum ($\sim 10^{-5}$–10^{-6} Torr) in a Lakeshore TTP6 cryogenic probe station.

As shown in Fig. 1(c), X-ray diffraction patterns of our SnS_2 and $SnSe_2$ samples can be indexed with hexagonal unit cells of the CdI_2-type, consistent with those reported.[21,22] For the solid solution compositions, the $SnS_{2-x}Se_x$ crystals also retain the CdI_2 structure type. As expected for a larger atomic radius of Se, the lattice constants determined from the XRD data increase with increasing Se content.

Figure 2 presents the electrical characteristics of a series of $SnS_{2-x}Se_x$ nanocrystal FETs, for which the thickness (in the order of 10 nm) and width of the conduction channels (nanocrystals) are listed in Table I (as determined by AFM). The drain-source current I_{DS} as a function of the gate voltage V_G at fixed drain-source voltage V_{DS} is plotted in Figs. 2(a)–2(f). For one of the end compounds, SnS_2 (Fig. 2(a)), a typical n-type behavior is observed as reported in our previous work.[15] The FET device is in a depleted state for negative V_G, and the current increases monotonically as V_G is swept to the positive side. This indicates that the device switches from a complete "OFF" state at negative V_G to an "ON" state at positive V_G (+50 V). When Se content is increased up to $x = 0.8$, similar n-type behaviors with a complete "OFF" state are observed (Figs. 2(b) and 2(c)). However, interestingly, at the Se content $x = 1.2$ and above (Figs. 2(d)–2(f)), a complete "OFF" state cannot be reached even with large negative Vg = −50 V, and the FET devices show a clearer tendency to saturate at the positive gate voltage (Fig. 2(d)). This observation suggests that for higher Se doping ($x \geq 1.2$) the FET conduction channel becomes heavily electron doped which may lead to a shift in the threshold voltage (V_t). This observation also indicates that the energy separation between the Fermi level (which is pinned near the impurity donor level for these n-type FETs) and the conduction-band minimum is reduced significantly with increasing Se content. Correspondingly, the number of thermally excited conduction electrons at room temperature increases with Se as we demonstrate it later with measurements of the activation energy of conductivity.

In Figs. 2(g)–2(l), the drain-source current I_{DS} as a function of drain-source voltage V_{DS} at fixed gate voltages $V_G = 0$ V and $V_G = +50$ V is presented. For SnS_2, $SnS_{1.6}Se_{0.4}$, $SnS_{1.2}Se_{0.8}$, and $SnS_{0.8}Se_{1.2}$, the asymmetry of the current-voltage curves observed at zero gate voltage can be explained in terms of an enlarged effective gate voltage between the drain and the gate electrode due to the applied V_{DS}.[15] In the low bias regions, the I-V curves are linear revealing low-barrier (nearly Ohmic) contacts for the FET devices based on $SnS_{2-x}Se_x$ with $x \leq 1.2$ (Figs. 2(g)–2(j)). In

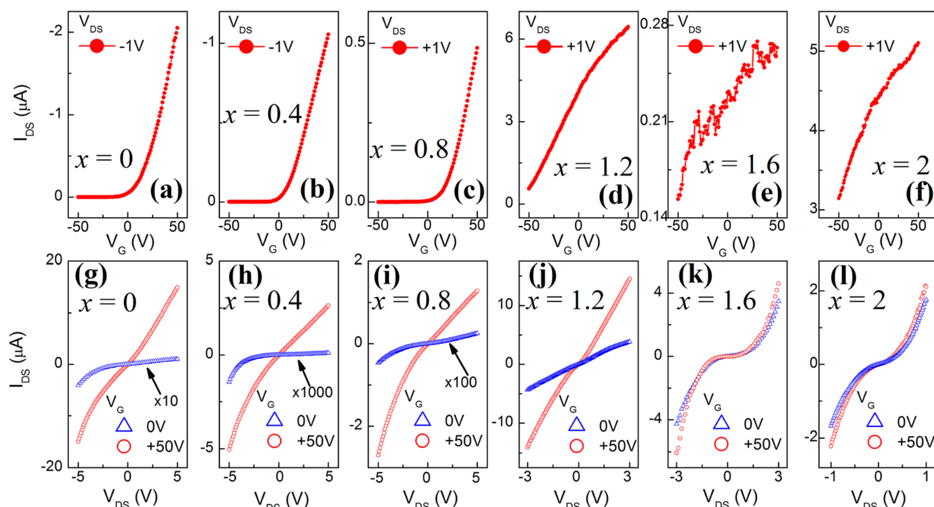

FIG. 2. (a)–(f): The drain-source current I_{DS} as a function of back gate voltage V_G (swept from −50 V to +50 V) at fixed drain-source bias voltage $|V_{DS}| = 1$ V for the FETs based on $SnS_{2-x}Se_x$ crystals with the Se composition x = 0, 0.4, 0.8, 1.2, 1.6, and 2.0 (consecutively, from left to right). (g)–(l): I_{DS} as a function of V_{DS} at fixed $V_G = 0$ V (triangles) and $V_G = +50$ V (circles) for the above $SnS_{2-x}Se_x$ devices with x = 0, 0.4, 0.8, 1.2, 1.6, and 2.0 (consecutively, from left to right). For clarity, the I_{DS} vs. V_{DS} curves at $V_G = 0$ are displayed by multiplying the actual I_{DS} values with a factor of 10, 1000, and 100, respectively, for the figures (g), (h) and (i).

TABLE I. The thickness and width of $SnS_{2-x}Se_x$ nanocrystals for the devices of Figs. 2 and 3.

Compounds	Thickness (nm)	Width (μm)
SnS_2	16	1.8
$SnS_{1.6}Se_{0.4}$	11	2.4
$SnS_{1.2}Se_{0.8}$	35	5.1
$SnS_{0.8}Se_{1.2}$	25	2.3
$SnS_{0.4}Se_{1.6}$	28	1.7
$SnSe_2$	25	1.3

contrast, for the FET devices with higher selenium concentrations ($SnS_{0.4}Se_{1.6}$ and $SnSe_2$), a non-linear I-V behavior is observed (Figs. 2(k) and 2(l)), which could be attributed to stronger Schottky barriers at the metal-semiconductor contacts. We note that this nonlinear I-V behavior is reproducibly observed in other FET devices with $x = 1.6$ and $x = 2.0$ and thus a higher Schottky barrier may be an intrinsic behavior for these doping levels. This could be related to the shift of the Fermi level in the high Se-content materials which can affect the formation of Schottky barrier, or due to the effect of surface states that influences the formation of Schottky barriers. We also note that the absolute magnitude of I_{DS} varies for devices shown in Fig. 2, because I_{DS} can be affected by many factors such as the contact barrier height, the detailed geometry of the $SnS_{2-x}Se_x$ crystal for each device, or a change in carrier density.

The I-V curves at gate voltage $V_G = 0\,V$ were also characterized with temperature varied from 90 K to 295 K, as shown in Figure 3. All SnS_xSe_{2-x}-based devices become less conductive with decreasing temperature, which is mostly due to the reduction of the number of thermally excited carriers. The conductivity activation energy, E_a, of the semiconducting FET channels can be determined from the temperature dependence of drain-source resistance, R, as given by the Arrhenius equation

$$R = R_0 e^{E_a/k_B T}, \quad (1)$$

where the R_0 is a pre-exponential constant factor, k_B is the Boltzmann constant, and T is the measurement temperature. The drain-source resistance R at different temperatures is determined by linear fitting of corresponding I-V curves at $V_{DS} = -1\,V$. The relationship of the FET channel composition with the obtained activation energy is plotted in Fig. 4(a).

The activation energy in a semiconductor can be expressed as

$$E_a = E_c - E_F, \quad (2)$$

where E_c is the conduction band minimum and E_F is the Fermi level. A comparison of the band gaps of the end-members, SnS_2 (2.1 eV) and $SnSe_2$ (1.0 eV), yields activation energies that are 1/15 th (SnS_2) and 1/54 th ($SnSe_2$) of their respective band gaps. This observation suggests that the Se-doping in $SnS_{2-x}Se_x$ leads to shallow donor impurities and the conductivity activation energy E_a should then be equal to the donor ionization energy, E_d.

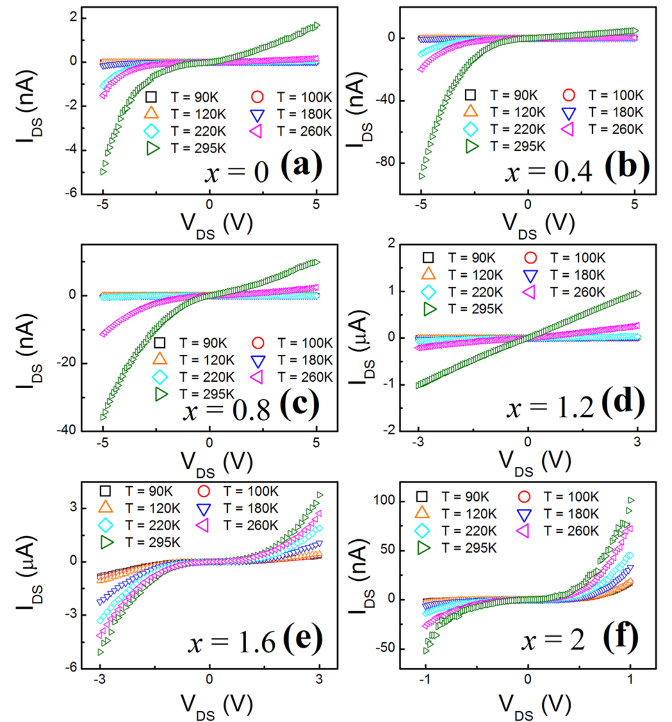

FIG. 3. I_{DS} vs. V_{DS} curves with $V_G = 0\,V$ measured at temperatures from 90 K to 295 K for the $SnS_{2-x}Se_x$ based FETs with x = 0, 0.4, 0.8, 1.2, 1.6, and 2.0 (consecutively, from (a) to (f)). Some curves at lower temperatures are nearly overlapping and indistinguishable in the plots. We note that low temperature experiments sometimes change the absolute value of I_{DS} significantly in such nano-scale FET devices, e.g., as can be seen from the data of Fig. 2(l) measured just before the cool down and those of Fig. 3(f) in the end of the low temperature experiment for the composition x = 2, probably due to changes in surface adsorption under different vacuum conditions and trapped charge states. However, the shape of IV curves is reproducible before and after the low temperature experiments for all compositions by comparing Figs. 2 and 3.

The simplest approach of calculating the ionization energies of shallow donors is to use a modified hydrogen-like model of impurities.[23] The energy of the first excited state E_d of an electron around a donor impurity is given by

$$E_d = -\frac{13.6}{\varepsilon_r^2}\frac{m_c^*}{m_0}\, eV, \quad (3)$$

where m_c^* is the effective mass of electron in the lowest conduction band, m_0 is that of a free electron at rest, and ε_r is the relative dielectric constant of the crystal host. Although Ref. 24 reports a conductivity effective mass $m_c^* = (0.4 \pm 0.2)\, m_0$ for $SnSe_2$ deduced from far-IR absorption measurements, there are no reports on directly measured m^* and ε_r for both SnS_2 and $SnSe_2$. Kramers-Kronig analysis of IR spectra of $SnSe_2$[25] yields a static dielectric constant of $\varepsilon_r(0) = 21.5$. Relevant data for SnS_2 are even scarcer. To overcome the lack of data needed for the estimation of ionization energies we performed density functional theory (DFT) calculations on the electronic band structure and dielectric properties of SnS_2 and $SnSe_2$.

DFT calculations on SnS_2 and $SnSe_2$ were performed using the generalized-gradient approximation (GGA) with Perdew-Wang (PW91) exchange-correlation functional, and the norm-conserved pseudopotential plane-waves as implemented in the Quantum Espresso suite.[26] The electronic band structure, related properties, and geometry optimization

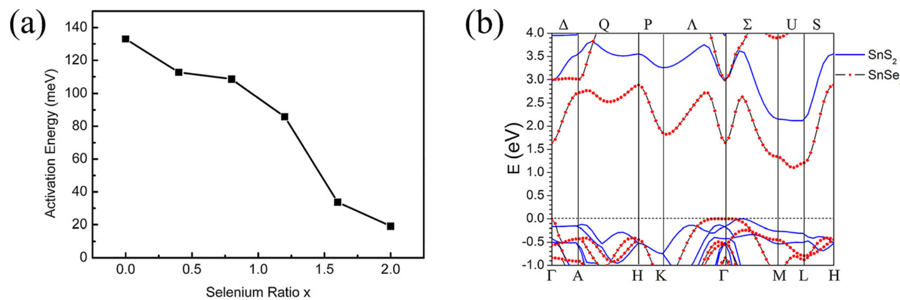

FIG. 4. (a) Activation energy at zero gate voltage as a function of selenium compositions (obtained by fitting the Arrhenius equation). (b) DFT calculated energy band structure of SnS_2 (solid line) and $SnSe_2$ (solid circles).

of the structures were calculated self-consistent (SCF) with 100 Ry kinetic energy cutoff for the plane wave, 400 Ry charge density cut-off, and SCF tolerance better than 10^{-8}. The DFT calculations yield an in-plane dielectric constant of $\varepsilon_r = 21.8$ for $SnSe_2$ that is surprisingly close to the experimental value reported in Ref. 25. This gives us confidence that the DFT value of $\varepsilon_r = 10.3$ for SnS_2 is reliable. More details on the DFT calculations on SnS_2 and $SnSe_2$ including phonons and lattice strain evolution in the mixed $SnS_{2-x}Se_x$ crystals are given in Ref. 27.

Fig. 4(b) presents the DFT electronic band dispersion curves along the high symmetry lines in the hexagonal Brillouin zone of SnS_2 (solid line) and $SnSe_2$ (solid circles). Here the Fermi energy ($E_F = 0$ eV) is set at the top of the valence band. The DFT values for the calculated indirect gaps of SnS_2 and $SnSe_2$ are 2.12 eV and 1.1 eV, respectively. These values are in good agreement with experiments.[17] Since the bottom of conduction band is at M-L (U-symmetry line), we focus on the isoenergy surfaces around the M and L points in k-space, as well as and along the U-line. The isoenergy surfaces in SnS_2 are found to be cylindrical, with axes along the U-line. This means that the electron effective mass at the bottom of conduction band of SnS_2, is highly anisotropic with a very large longitudinal component $m_l^* \gg m_0$ along M-L (or the c-axis) and a transversal (in-plane) component $m_t^* = 1.097\, m_0$. For $SnSe_2$, the anisotropy is weaker and one finds $m_l^* = 1.571\, m_0$ and $m_t^* = 0.732\, m_0$. Having considered the anisotropy of SnS_2 and $SnSe_2$, the conductivity effective mass m_c^* is then given by

$$m_c^* = 3\left(\frac{1}{m_l^*} + \frac{2}{m_t^*}\right)^{-1}. \quad (4)$$

Using Eq. (4), the calculated DFT conductivity effective masses are $1.646\, m_0$ (SnS_2) and $0.889\, m_0$ ($SnSe_2$). Therefore, the corresponding donor ionization energies calculated with Eq. (3) are 210 meV and 25.5 meV for SnS_2 and $SnSe_2$, respectively. The above calculated values for E_d (which is equal to E_a) are consistent with the experimentally observed trend of decreasing excitation energy E_a with increasing selenium composition (x) (Fig. 4(a)). However the theoretical values seem to overestimate those measured in this work.

From these estimates we can conclude, without making DFT calculations for the mixed $SnS_{2-x}Se_x$, that these compounds inherently contain donor impurities, either S(Se) vacancies or possibly iodine atoms (accompanying the chemical vapor transport crystal growth). Donor ionization energies depend mostly on the dielectric properties of the host crystal, which in turn reflect the band structure and specifically the band gap. As the band gap decreases, the screening of electric field is attenuated, and the ionization energy of the same type donor impurities decreases.

In summary, the field-effect devices were fabricated using thin crystals of tin dichalcogenides $SnS_{2-x}Se_x$ with varying Se-content (x). Increasing Se content results in a reduction of the band gap. This is accompanied by an increase in dielectric constant and a corresponding decrease of the donor ionization energy. The Fermi energy is shifted closer to the conduction band minimum (i.e., the activation energy E_a decreases) as the Se composition is increased, and thus the drain-source current modulation is suppressed. This study will be instructive and useful for future application of tin dichalcogenides in nanoelectronics.

This work was supported by the National Science Foundation (ECCS-1247874 monitored by Anupama Kaul), and the State of Texas through the Texas Center for Superconductivity (TcSUH) at the University of Houston. J.M. and A.M.G. also acknowledge the support from the R. A. Welch Foundation (E-1297).

[1]K. S. Novoselov, A. K. Geim, S. V. Morozov, D. Jiang, Y. Zhang, S. V. Dubonos, I. V. Grigorieva, and A. A. Firsov, Science **306**, 666 (2004).
[2]K. S. Novoselov, A. K. Geim, S. V. Morozov, D. Jiang, M. I. Katsnelson, I. V. Grigorieva, S. V. Dubonos, and A. A. Firsov, Nature **438**, 197 (2005).
[3]A. K. Geim and K. S. Novoselov, Nature Mater. **6**, 183 (2007).
[4]A. H. C. Neto, F. Guinea, N. M. R. Peres, K. S. Novoselov, and A. K. Geim, Rev. Mod. Phys. **81**, 109 (2009).
[5]C. Soldano, A. Mahmood, and E. Dujardin, Carbon **48**, 2127 (2010).
[6]K. S. Novoselov, D. Jiang, F. Schedin, T. J. Booth, V. V. Khotkevich, S. V. Morozov, and A. K. Geim, Proc. Natl. Acad. Sci. U.S.A. **102**, 10451 (2005).
[7]A. Ayari, E. Cobas, O. Ogundadegbe, and M. S. Fuhrer, J. Appl. Phys. **101**, 014507 (2007).
[8]Q. H. Wang, K. Kalantar-Zadeh, A. Kis, J. N. Coleman, and M. S. Strano, Nat. Nanotechnol. **7**, 699 (2012).
[9]S. Balendhran, J. Deng, J. Z. Ou, S. Walia, J. Scott, J. Tang, K. L. Wang, M. R. Field, S. Russo, S. Zhuiykov, M. S. Strano, N. Medhekar, S. Sriram, M. Bhaskaran, and K. Kalantar-zadeh, Adv. Mater. **25**, 109 (2013).
[10]D. B. Mitzi, L. L. Kosbar, C. E. Murray, M. Copel, and A. Afzali, Nature **428**, 299 (2004).
[11]H. T. Yuan, M. Toh, K. Morimoto, W. Tan, F. Wei, H. Shimotani, C. Kloc, and Y. Iwasa, Appl. Phys. Lett. **98**, 012102 (2011).
[12]T. Kyratsi, K. Chrissafis, J. Wachter, K. M. Paraskevopoulos, and M. G. Kanatzidis, Adv. Mater. **15**, 1428 (2003).
[13]S.-G. Hur, E.-T. Kim, J.-H. Lee, G.-H. Kim, and S.-G. Yoon, J. Vac. Sci. Technol. B **26**, 1334 (2008).
[14]B. Li, J. Liu, G. Xu, R. Lu, L. Feng, and J. Wu, Appl. Phys. Lett. **101**, 153903 (2012).
[15]D. De, J. Manongdo, S. See, V. Zhang, A. Guloy, and H. Peng, Nanotechnology **24**, 025202 (2013).
[16]International Technology Roadmap for Semiconductors (ITRS), Emerging Research Devices (ERD), 2011 edition, 2012.
[17]C. Julien, M. Eddrief, I. Samaras, and M. Balkanski, Mater. Sci. Eng., B **15**, 70 (1992).

[18]G. Perluzzo, S. Jandl, M. Aubin, and P. E. Girard, Solid State Commun. **27**, 1437 (1978).
[19]R. H. Williams, R. B. Murray, D. W. Govan, J. M. Thomas, and E. L. Evans, J. Phys. C **6**, 3631 (1973).
[20]F. A. S. Al-Alamy and A. A. Balchin, J. Cryst. Growth **38**, 221 (1977).
[21]J. R. Guenter and H. R. Oswald, Naturwiss. **55**, 177 (1968).
[22]B. Palosz and E. Salje, J. Appl. Crystallogr. **22**, 622 (1989).
[23]C. Kittel, *Introduction of Solid State Physics*, 4th ed. (John Wiley & Sons, New York, 1986), p. 206.
[24]P. A. Lee and G. Said, J. Phys. D: Appl. Phys. **1**, 837 (1968).
[25]Landolt-Börnstein—Group III, *Condensed Matter* (Springer, 1998), Vol. 41C, pp. 1–6.
[26]G. Paolo, B. Stefano, B. Nicola, C. Matteo, C. Roberto, C. Carlo, C. Davide, L. C. Guido, C. Matteo, D. Ismaila, C. Andrea Dal, G. Stefano de, F. Stefano, F. Guido, G. Ralph, G. Uwe, G. Christos, K. Anton, L. Michele, M.-S. Layla, M. Nicola, M. Francesco, M. Riccardo, P. Stefano, P. Alfredo, P. Lorenzo, S. Carlo, S. Sandro, S. Gabriele, P. S. Ari, S. Alexander, U. Paolo, and M. W. Renata, J. Phys. Condens. Matter **21**, 395502 (2009).
[27]V. G. Hadjiev, D. De, H. B. Peng, J. Monongdo, and A. M. Guloy, Phys. Rev. B **87**, 104302 (2013).